Lateral shearing interferometry of high-harmonic wavefronts

Dane R. Austin,[1,3,*] Tobias Witting,[1,2] Christopher A. Arrell,[2] Felix Frank,[2] Adam S. Wyatt,[1] Jon P. Marangos,[2] John W.G. Tisch,[2] and Ian A. Walmsley[1]

[1]*Clarendon Laboratory, University of Oxford, Parks Road, Oxford, OX1 3PU, UK*

[2]*Quantum Optics and Laser Science Group, Blackett Laboratory, Imperial College London, London SW7 2BW, UK*

[3]*Currently at ICFO–Institut de Ciencies Fotoniques, Mediterranean Technology Park, 08860 Castelldefels (Barcelona), Spain*

**Corresponding author: dane.austin@icfo.es*

Received February 3, 2011; revised March 28, 2011; accepted March 31, 2011;
posted March 31, 2011 (Doc. ID 142129); published May 4, 2011

We present a technique for frequency-resolved wavefront characterization of high harmonics based on lateral shearing interferometry. Tilted replicas of the driving laser pulse are produced by a Mach–Zehnder interferometer, producing separate focii in the target. The interference of the resulting harmonics on a flat-field extreme ultraviolet spectrometer yields the spatial phase derivative. A comprehensive set of spatial profiles, resolved by harmonic order, validate the technique and reveal the interplay of single-atom and macroscopic effects. © 2011 Optical Society of America

OCIS codes: 120.5050, 020.2649, 190.2620, 340.7450, 120.3180.

The space–time structure of radiation produced by high-harmonic generation (HHG) contains signatures of both the angstrom-sized spatial features and attosecond scale temporal features of the response of single atoms to the strong driving field [1], as well as the macroscopic effects of propagation through the ensemble of atoms [2]. Decoding these signatures from the complex spatio–temporal profile of the generated extreme ultraviolet (XUV) and soft x-ray fields is important both for unraveling the physical processes involved in the atomic response, as well as for optimizing HHG for applications such as attosecond pump probe experiments[3], imaging [4], and seeding free-electron lasers [5]. The possibility that significant space–time coupling may be present in HHG means that full multidimensional characterization can be necessary. Temporal field profiles measured at a single spatial point or averaged over the beam, or vice versa, will be inadequate in many cases. Most phase-sensitive diagnostics do not satisfy this requirement: temporal reconstructions based on photoelectron spectroscopy average over all points in the beam, while spatial wavefront measurements based on point-diffraction interferometry [6] or a Shack–Hartmann wavefront sensor [7] average over frequencies.

Recently, a frequency-resolved wavefront measurement was demonstrated using the spectral wavefront optical reconstruction by diffraction (SWORD) method: the diffraction pattern from a slit placed near the focus of the harmonic beam is monitored on a flat-field XUV spectrometer [8]. Such a measurement offers much useful information: differences in the wavefront curvature of the harmonics are relevant for focusing attosecond pulses and seeding tunable free-electron lasers, and it may be combined with a single temporal measurement to return the full spatio–temporal profile. However, some potential disadvantages of SWORD are its inherently scanning nature and the attenuation caused by the slit, which must be narrower than the spatial features of the beam.

Here we present an approach based on lateral shearing interferometry (LSI), which overcomes these issues. We compare simulations with experimentally obtained spatial phase and amplitude profiles. We obtain good agreement, validating the method, and our measurements reveal the interplay of the single-atom response and the propagating wavefront of the laser.

The experimental setup, depicted in Fig. 1, is similar to that of previous interferometric diagnostics of HHG [9]. The laser pulses pass through a Mach–Zehnder interferometer aligned to produce output with approximately zero delay, a small (compared to the beam size) relative displacement, and a tilt between the beams. The displacement and tilt are in the horizontal plane. Arm A remains stationary throughout, while roof-hat mirror pair in arm B is laterally displaced a distance, x_r. The beams are focused by optic F, which in our experiment is an off-axis parabolic mirror, onto the target, T. Owing to the tilt, they form separate focii, each of which undergoes HHG. The harmonics propagate to a flat-field XUV spectrometer consisting of a slit S, a grating G, and a two-dimensional detector D. The spectrometer disperses the harmonics vertically; in the horizontal plane they undergo free propagation and overlap, forming a two-source spatial interference pattern with carrier $K = sk/L$, where $s = 130\,\mu$m is the focii separation, $k = \omega/c$ is the free-space wavenumber of the harmonics, and $L = 118$ cm is the distance from the focal plane to the detector. Translations of the B arm of the interferometer displace the harmonics on the detector a distance $x_d = 2Lx_r/f$,

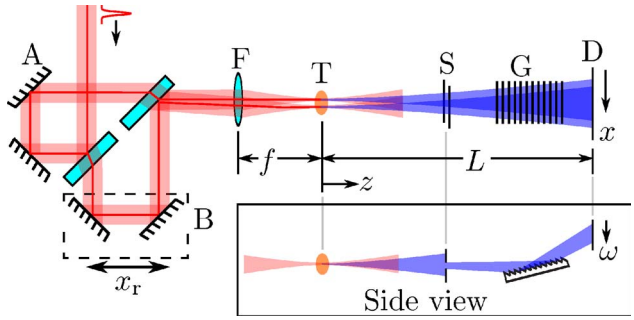

Fig. 1. (Color online) Top and side (inset) views of the setup. The symbols are explained in the text.

where $f = 40\,\mathrm{cm}$ is the focal length. The modulation of interferogram fringes is proportional to $\cos\Phi(x,\omega;x_\mathrm{d})$, where

$$\Phi(x,\omega;x_\mathrm{d}) = \phi_\mathrm{B}(x - x_\mathrm{d},\omega) + \frac{x_\mathrm{d}kx}{L} + Kx - \phi_\mathrm{A}(x,\omega). \tag{1}$$

Here, $\phi_\mathrm{A}(x,\omega)$ and $\phi_\mathrm{B}(x,\omega)$ are the phases of the harmonics from arms A and B, respectively, at the detector plane. The second term on the right-hand side of Eq. (1) represents the change in tilt of the harmonic beams caused by the action of the focusing optic upon a lateral displacement. A typical raw interferogram is shown in Fig. 2(a). The Fourier domain filtering algorithm [10] is used to isolate the sidebands whose phase is $\Phi(x,\omega;x_\mathrm{d})$. Since the frequency dependence of the carrier K is significant for broadband harmonic fields, we obtain optimal noise rejection by performing a discrete Fourier transform (DFT) along x and applying a frequency-dependent passband filter, as shown by the red curves in Fig. 2(b). We also perform low-pass filtering (not shown) along the frequency axis (vertical in Fig. 2). A typical sideband phase $\Phi(x,\omega;x_\mathrm{d})$ is shown in Fig. 2(c). If x_d and K are known, and the A and B fields are identical, then the phase of the harmonics may be retrieved from $\Phi(x,\omega;x_\mathrm{d})$ by the usual concatenation procedure for shearing interferometry [11]. However, the sensitivity of HHG is such that producing two identical sources is difficult, and we therefore use a multiple-shot method that avoids this requirement. One records and filters interferograms at two different displacements, $x_{\mathrm{d},1}$ and $x_{\mathrm{d},2}$. Subtracting the extracted phases yields

$$\begin{aligned}\Gamma(x,\omega;X_\mathrm{d}) &= \Phi(x + x_{\mathrm{d},1},\omega;x_{\mathrm{d},2}) - \Phi(x + x_{\mathrm{d},1},\omega;x_{\mathrm{d},1}) \\ &= \phi_\mathrm{B}(x + X_\mathrm{d},\omega) - \phi_\mathrm{B}(x,\omega) - \frac{X_\mathrm{d}kx}{L}.\end{aligned} \tag{2}$$

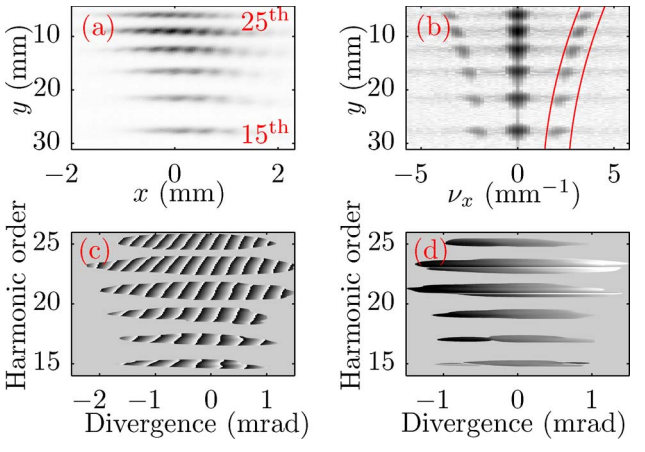

Fig. 2. (Color online) Processing steps. (a) Raw data, linear gray scale. The 15th and 25th harmonics are labeled for reference. (b) Horizontal DFT of raw data, logarithmic gray scale with 10^{-6} amplitude dynamic range, ν_x is spatial frequency in x. The red curves indicate the filter passband. (c) Interferogram phase, $[-\pi,\pi]$ rad linear gray scale. (d) Phase difference between two interferograms, $[-5,5]$ rad linear gray scale. In (c) and (d), regions of low signal to noise ratio are set to a constant value.

A typical result for $\Gamma(x,\omega;X_\mathrm{d})$ is shown in Fig. 2(d). Equation (3) constitutes a spectrally resolved LSI measurement of the field B at the detector plane with shear $X_\mathrm{d} = x_{\mathrm{d},1} - x_{\mathrm{d},2}$. The third term in Eq. (3) arises from the tilt and gives a quadratic contribution $\phi_\mathrm{p} = -\frac{kx^2}{2L}$. This is the opposite of the phase of a point source diffracting into a spherical wave (within the paraxial approximation) over a distance L. It therefore cancels out the predominately quadratic phase caused by propagation of the harmonics to the detector, leaving only the deviation of the harmonics from an ideal point source in the focal plane of F.

If the focus-detector distance L is sufficiently large that the Fraunhofer diffraction approximation applies, then Eq.(3) may be rewritten as

$$\Gamma(x,\omega;X_\mathrm{d}) = \tilde{\phi}_\mathrm{B}\left(k\frac{x + X_\mathrm{d}}{L},\omega\right) - \tilde{\phi}_\mathrm{B}\left(k\frac{x}{L},\omega\right), \tag{3}$$

where $\tilde{\phi}_\mathrm{B}(k_x,\omega)$ is the phase of the spatial Fourier transform of the field in the focal plane of F. Equation (3) represents LSI of the spatial Fourier transform of the B arm harmonics, with wavenumber shear $K_\mathrm{d} = kX_\mathrm{d}/L$. We shall henceforth refer to the focal plane of F as the near field and its spatial Fourier transform as the far field. For reconstruction we use a multiple-shear concatenation algorithm, simplified from the general case [11] because there are no intensity nulls in the profiles.

Using the new method, we measured the spatial profiles of harmonics 13–25 of a 14 fs Ti:sapphire pulse in a 1.25 mm (zero-to-zero) thick 0.1 atm krypton pulsed-valve gas jet. The laser peak intensity was $1.4\times10^{14}\,\mathrm{W/cm^2}$ and the waist size was $50\,\mu\mathrm{m}$ (intensity e^{-2} radius). To verify our results and gain insight into the physics, we performed a corresponding set of simulations. We used an adiabatic quantum orbits model [12]. All of the simulation parameters were consistent with experimental values. We approximated the longitudinal density profile of the gas jet as cosine-squared. The simulations predicted a maximum estimated ionization fraction of 2%. Although the induced defocusing influenced the spatial profiles it did not qualitatively affect the trends described below. The phase-matching response was dominated by neutral gas dispersion and absorption, with the intensity dependence of the single-atom response, the plasma-induced dephasing, and the Gouy phase playing comparatively minor roles. Therefore, both short and long trajectories were predicted, but the broader angular distribution of the latter [2] meant that their intensity was largely below the experimental sensitivity.

Figure 3 shows the far-field profiles for several harmonics with the gas jet at the focus. Over regions of significant intensity, the agreement of the experimental phase with the simulations is good. The broadening of the far-field intensity profiles with harmonic order is partly due to the higher harmonics having a higher cutoff, and, hence, a narrower (broader) near- (far-) field distribution. These facts do not explain the far-field phase profiles, which have negative curvature for the higher harmonics but are nearly flat for the lower harmonics. The variation is due to the intensity-dependent dipole phase, which arises from the electron's sojourn in the continuum [2]. For the short trajectories, this intensity

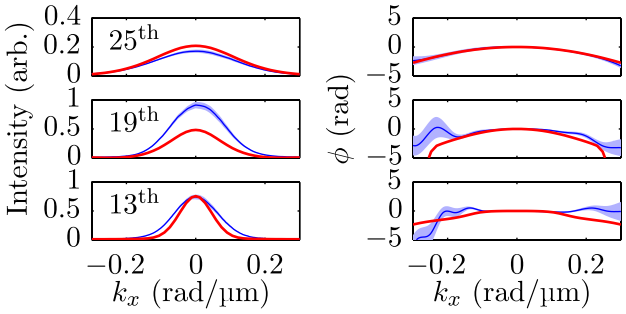

Fig. 3. (Color online) Far-field intensity (left column) and phase (right column) of the 13th, 19th, and 25th harmonics (indicated at top-left), showing experiment (blue, thinner curve, uncertainty represented by shaded region) and simulation (red, thicker curve).

dependence increases with harmonic order, so that lower harmonics have a flat near- and far-field phase, while higher harmonics have positive (negative) phase curvature in the near (far) fields. The phase of the lower harmonics exhibits slope changes in the wings, which lie below the sensitivity of our experiment. Our simulations indicate that these arise from the long trajectories.

We also studied the dependence of the far-field profiles on the position of the gas jet. Since they are close to Gaussian, they are fully described by their intensity e^{-1} radius σ_{k_x}, and phase curvature ϕ_{2,k_x}, presented in Fig. 4 for the 25th harmonic. Although there is some disagreement with the simulation, it is present in the intensity as well as the phase profiles. This suggests that it results from the simplicity of our model and a non-Gaussian beam profile in our experiment, rather than erroneous phase measurements. We observe identical trends, which result from the interplay of the phase of the laser wavefront with the intensity-dependent atomic dipole phase. For the gas jet before the focal plane ($z < 0$), the laser wavefront is converging, i.e., it has negative curvature, which tends to cancel the intensity-dependent dipole phase. The near-field phase is therefore flat. This results in a narrow far-field profile with low phase curvature. As the gas jet moves through the focus, the laser wavefront changes to diverging and acts in concert with the intensity-dependent dipole phase to produce a large near-field phase curvature. This broadens the far-field profile, and initially ($z \approx -2$ mm) produces a large far-field phase curvature. Subsequent increase in the near-field curvature decreases the far-field curvature, as may be understood from the properties of chirped Gaussian pulses upon Fourier transformation.

We have shown that even in this relatively simple regime of an atomic gas with low ionization levels, there are some subtle effects of which spectrally resolved wavefront sensing is necessary for direct observation. In this Letter we have robustly demonstrated a method for achieving this task. For molecular targets and higher laser intensities, it may be expected that complexity will only increase. For example, ionization-induced

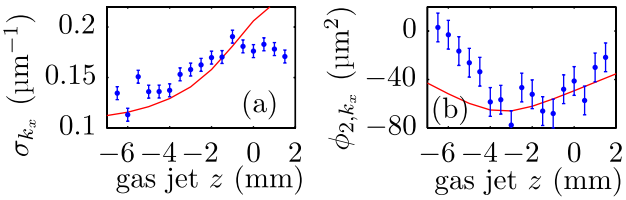

Fig. 4. (Color online) (a) Width and (b) spatial phase curvature of measured (blue dots) and simulated (red curve) far-field profiles of the 25th harmonic versus gas jet z position with respect to the focus.

defocusing will superpose an additional imprint on the spatial phase. Understanding the phenomena that arise will not only be of interest for fundamental science, but will assist in exploiting the full potential of HHG.

The authors thank J. S. Robinson. The Engineering and Physical Sciences Research Council (EPSRC) grants EP/H000178/1, EP/F034601/1, and EP/E028063/1, and the European Union (EU) grant PITN-GA-2008-214962 supported this work. I. Walmsley was supported by the Royal Society. A. Wyatt was supported by the Leverhulme Trust (F/08776/C).

References

1. F. Krausz and M. Ivanov, Rev. Mod. Phys. **81**, 163 (2009).
2. M. B. Gaarde, J. L. Tate, and K. J. Schafer, J. Phys. B **41**, 132001 (2008).
3. G. Sansone, F. Kelkensberg, J. F. Pérez-Torres, F. Morales, M. F. Kling, W. Siu, O. Ghaur, P. Johnsson, M. Swoboda, E. Benedetti, F. Ferrari, F. Lépine, J. L. Sanz-Vicario, S. Zherebtsov, I. Znakovskaya, A. L'Huillier, M. Y. Ivanov, M. Nisoli, F. Martín, and M. J. J. Vrakking, Nature **465**, 763 (2010).
4. R. L. Sandberg, A. Paul, D. A. Raymondson, S. Hädrich, D. M. Gaudiosi, J. Holtsnider, R. I. Tobey, O. Cohen, M. M. Murnane, H. C. Kapteyn, C. Song, J. Miao, Y. Liu, and F. Salmassi, Phys. Rev. Lett. **99**, 098103 (2007).
5. G. Lambert, T. Hara, D. Garzella, T. Tanikawa, M. Labat, B. Carre, H. Kitamura, T. Shintake, M. Bougeard, S. Inoue, Y. Tanaka, P. Salieres, H. Merdji, O. Chubar, O. Gobert, K. Tahara, and M.-E. Couprie, Nat. Phys. **4**, 296 (2008).
6. D. G. Lee, J. J. Park, J. H. Sung, and C. H. Nam, Opt. Lett. **28**, 480 (2003).
7. C. Valentin, J. Gautier, J.-P. Goddet, C. Hauri, T. Marchenko, E. Papalazarou, G. Rey, S. Sebban, O. Scrick, P. Zeitoun, G. Dovillaire, X. Levecq, S. Bucourt, and M. Fajardo, J. Opt. Soc. Am. B **25**, B161 (2008).
8. E. Frumker, G. G. Paulus, H. Niikura, D. M. Villeneuve, and P. B. Corkum, Opt. Lett. **34**, 3026 (2009).
9. M. Bellini, C. Lyngå, A. Tozzi, M. B. Gaarde, T. W. Hänsch, A. L'Huillier, and C.-G. Wahlström, Phys. Rev. Lett. **81**, 297 (1998).
10. M. Takeda, H. Ina, and S. Kobayashi, J. Opt. Soc. Am. **72**, 156 (1982).
11. D. R. Austin, T. Witting, and I. A. Walmsley, J. Opt. Soc. Am. B **26**, 1818 (2009).
12. L. E. Chipperfield, P. L. Knight, J. W. G. Tisch, and J. P. Marangos, Opt. Commun. **264**, 494 (2006).